

Growth Morphology and Spectroscopy of Multiwall Carbon Nanotubes Synthesized by Pyrolysis of Iron Phthalocyanine

Rodrigo A. Segura, Wladimir Ibáñez, Rodrigo Soto, Samuel Hevia, and Patricio Häberle*

Departamento de Física, Universidad Técnica Federico Santa María, Avenida España 1680, 2391206 Valparaíso, Chile

Carbon nanotubes (CNTs) were synthesized by Chemical Vapor Deposition (CVD) from the pyrolytic decomposition of Iron Phthalocyanine (FePc) molecules, on SiO₂/Si(111) substrates in the presence of a hydrogen flow. FePc molecules contribute simultaneously both to the formation of the precursor Fe nanoparticles and also as a Carbon source. Different experimental conditions were examined. Samples were characterized by scanning electron microscopy, transmission electron microscopy, Raman spectroscopy, X-ray photoelectron spectroscopy, and inverse photoemission. The resulting samples are highly oriented multiwall carbon nanotubes films, with heights in the range between: 4 and 20 μm. The tubes diameter is strongly dependent on growth temperature. Our experimental results show evidence of a transition in the growth mechanism, from a tip growth to a base growth mode, as the decomposition temperature is increased. Preliminary spectroscopic measurements performed on these MWCNTs, show the unoccupied density of states has several resonances close to Fermi level, related both to the graphene electronic structure and the formation of the tube.

Keywords: Carbon Nanotubes, MWCNTs, CVD, Inverse Photoemission.

1. INTRODUCTION

Since their discovery,¹ the design and study of carbon nanotubes (CNTs), nanotubes-based materials and devices have become topics of great interest in material science. CNTs have been used as building blocks in the design of molecular electronic devices of great technological interest,^{2,3} as field emitters, in diodes, transistors, flat-panel displays, scanning probe microscopy tips, and many others. Potential applications currently being investigated include hydrogen storage, reinforced polymers, molecular (drug) delivery, and scaffolding in tissue engineering.

It is known that CNTs grown by chemical vapor deposition (CVD) methods nucleate around metallic particles. The most commonly used have been: Fe, Co, and Ni.⁴⁻⁷ Nanoparticles of these metals can serve as catalyst in the decomposition of hydrocarbonated molecules and induce the growth of the CNTs. The metal nanoparticles are generally deposited on a flat crystalline substrate like silicon, or supported in porous oxides like alumina or silica.⁵ In many cases organometallic precursors, like metallocenes and metal phthalocyanines (Metal Organic CVD), have been used to induce the formation of the nanoparticles within the CVD reactor. The C atoms source is the same

organometallic compound or alternatively they are fed as an organic gas flow, such as methane, ethane, acetylene, xylene, or toluene among others.⁴ The decomposition of the carbon source takes place generally at temperatures between 500 and 1000 °C, usually in the presence of molecular hydrogen which also contributes to the formation of the metallic nanoparticles in the case of the organometallic precursor. If the particles have been previously deposited on a substrate, hydrogen helps in their catalytic activation.

Due to the importance of the physical dimensions of these singular objects, the knowledge and manipulation of their size, structure, and crystalline order, among others plays a fundamental role in many applications. The control of these parameters could be attained by modifying experimental conditions such as growth temperature, gas flow, catalyst particle size, and constituents, carbon source, type of substrate and amount of reactants, among others.

This report is focused on the synthesis of well oriented CNTs samples, grown vertically on SiO₂/Si substrates, using Chemical Vapor Deposition methods (CVD), with the purpose of manufacturing samples which could be characterized by electron spectroscopy. The information about the electronic structure provided by these techniques is extremely valuable for many applications. Surface science techniques, which render information about the

*Author to whom correspondence should be addressed.

electronic structure of a system, ideally require: Flat surfaces, single domains, and good crystalline order, to enable the extraction of meaningful information. Maximizing uniformity and both reducing and quantifying the density of defects, together with understanding their effect on the measured physical variables, is still a pending challenge in the case of CNTs.

We have chosen the thermal decomposition of Iron(II) Phthalocyanine (FePc) as the synthesis method. As described before, this compound has the double role of supplying the Fe atoms for the formation of the metallic nanoparticles and as a carbon source, providing the atoms for the nanotube walls.

There are several reports of FePc related CNTs synthesis.^{8,9} Based on these results and our experience, a general model for the synthesis process can be proposed: The FePc molecules are decomposed in presence of molecular hydrogen, a redox reaction takes place, which induces the formation of metallic Fe atoms. Clustering of Fe atoms over the supporting surfaces yields nanoparticles (Fe-NPs). These Fe-NPs grow and disperse on the substrate and reactor walls. On the other hand, hydrocarbon fragments formed during this cracking reaction are recombined with the Fe nucleus to form a graphitic structure on their surface. Continuously, carbon atoms from the surrounding hydrocarbonated gas dissolve into the Fe-NPs and diffuse to the NP interface where they assemble into different carbon nanostructures. As more carbon atoms are incorporated, a C shell-like structure is extruded from the NPs. The extrusion force,¹⁰ takes off the graphitic hemisphere covering the NP to form a cylindrical structure, which grows preferentially away from the substrate surface. Hence the Fe nucleus behaves as a seed in the CNTs growth process.

Even though previous results are similar to ours, we have explored a wider range of experimental conditions, flow rates, temperatures, and growth times to determine their effect on the final products. In addition we show a complete characterization of the CNT film morphologies and correlate them with the experimental growth conditions.

2. EXPERIMENTAL DETAILS

2.1. Materials

Commercially available FePc^{11a} was used without further purification. The substrates were high purity Si(111) wafers^{11b} ($\sim 1 \times 1 \text{ cm}^2$). They were cleaned first with a piranha solution ($\text{H}_2\text{SO}_4:\text{H}_2\text{O}_2$, 7:3) to remove organic contaminants and subsequently rinsed with de-ionized water. A brief immersion (15 s) in HF (10%) was used to remove the native oxide layer. The Si samples were subsequently thermally oxidized at 1100 °C for 36 min, to form an approximate 100 nm thick oxide layer.^{11d} Argon, oxygen, and hydrogen used in this process, were nominally extra pure grades (99.998%, 99.5%, and 99.995%, respectively).

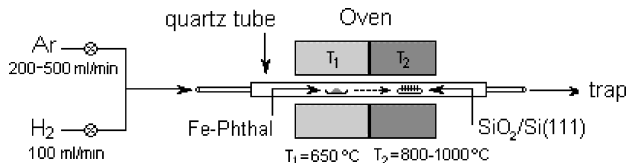


Fig. 1. Chemical Vapor Deposition system as set up for the synthesis of CNTs.

2.2. Chemical Vapor Deposition Setup

The CVD system consists of a horizontal two-stage furnace fitted with a quartz tube (33 mm ID) and various stainless steel gas flow lines, as shown in Figure 1. Argon and hydrogen gases were fed into the system using flow regulators.

2.3. Nanotubes Growth

In a typical reaction, 0.05 g of Iron(II) Phthalocyanine, $\text{Fe}(\text{C}_{32}\text{H}_{16}\text{N}_8)$, were deposited in a quartz boat located in the first stage of the oven. The $\text{SiO}_2/\text{Si}(111)$ wafers were placed in the second stage. This second stage was programmed to temperatures in the range between 800 to 1000 °C. The gases: Argon (200, 500 ml/min) and hydrogen (100 ml/min), were fed through the gas flux lines into the oven first stage. The furnace was initially purged with Ar. The exhaust gases were bubbled through a Glycerin trap into the atmosphere. Once the set point has been reached in the growth chamber, the temperature is raised to 650 °C in the furnace first stage. At 650 °C FePc molecules are sublimed and transported through the quartz tube by the carrier gas. The decomposition of the molecules takes place in the second section of the furnace. The “growth time” was measured from the instant the first stage reaches 650 °C. Under these conditions the typical reaction time was 20 min.

2.4. Characterization Techniques

Scanning Electron Microscopy (SEM) characterization was performed on the as prepared samples. The analysis was carried out in a LEO SEM model 1420VP operated between 10–20 KV. Conventional Transmission Electron Microscopy (TEM) measurements were performed on dispersed samples. For these studies, a drop of the dispersed CNTs was left to dry out on a commercial carbon coated Cu grids.^{11c} The bright field micrographs were taken in a Zeiss EM 900 operated between 50 and 80 KV. Raman spectroscopy was performed in a LabRam 010 Spectrophotometer. The spectra were collected between 100 and 2000 cm^{-1} . Inverse photoemission spectroscopy (IPS) was performed in a home built isochromat spectrometer.¹² XPS measurements were performed in a separate vacuum system, with an Al anode X-ray source and a hemispherical electron analyzer.

3. RESULTS AND DISCUSSION

Samples were synthesized at three different decomposition temperatures, 800, 900, and 1000 °C, with Argon flows of 1000, 500, and 200 ml/min. Other experimental parameters such as the H₂ flow (100 ml/min) were kept constant. The resulting products include the formation of CNTs densely packed, with a preferential orientation perpendicular to the substrate surface, as can be seen in the SEM micrographs of Figures 2 and 3. Collectively, the CNTs form a film of constant thickness resembling a turf or carpet over the smooth substrate.⁹ As could be foreseen, the CNTs not only grow on the substrates, but also on the reactor inside walls and substrate holder boats. The use of flat thermal Si oxide substrates allows the formation of the vertically aligned CNTs array.

Figure 2 corresponds to tubes grown with an Ar flow of 500 ml/min whereas Figure 3 shows similar images from CNTs synthesized at 200 ml/min. From the SEM micrographs it is possible to obtain some conclusions about the synthesis process. The reactor temperature influences considerably the length of the CNTs. For those grown at 1000 °C (Ar-500 ml/min), the average tube length was 13 μm and for those synthesized at 900 °C, the average length was only 6 μm. A similar result was obtained for

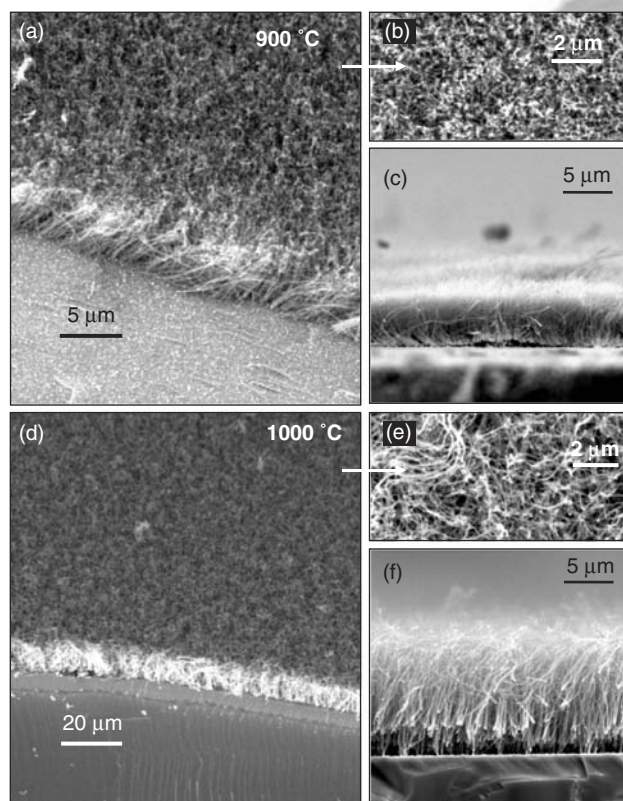


Fig. 2. SEM images of CNTs films synthesized with an Argon flux of 500 ml/min. The samples were grown for 20 min at 900 °C (a–c) and 1000 °C (d–f). In (a) we have physically removed part of the film, inducing some local disorder, to expose the substrate. The white speckles on the substrate are the Fe-NPs.

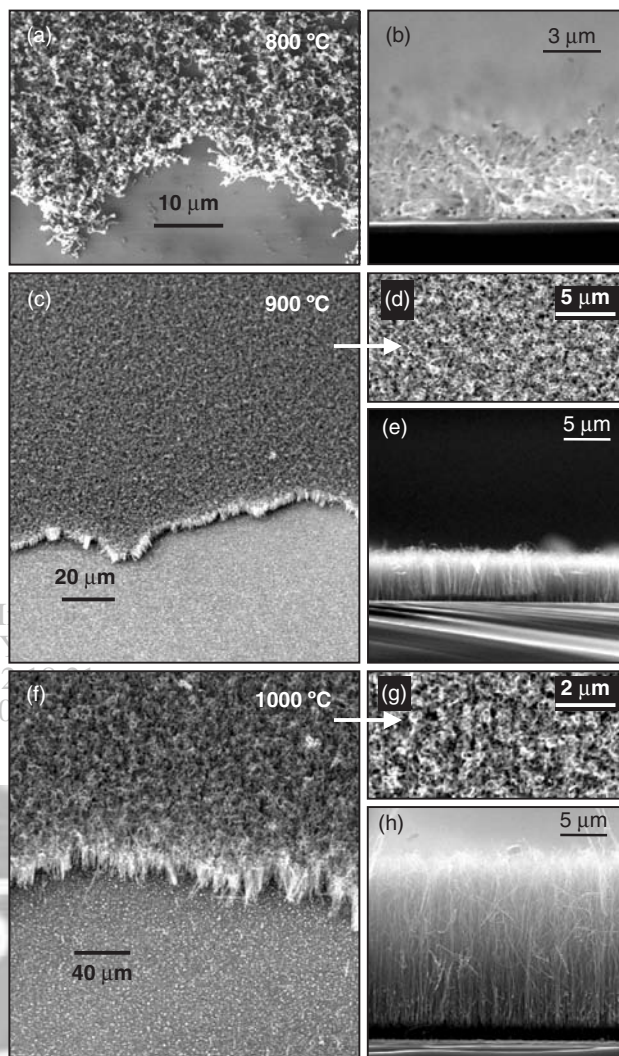


Fig. 3. SEM images of CNTs films synthesized with an Argon flow of 200 ml/min. The samples were grown at 800 °C (a, b), 900 °C (c–e), and 1000 °C (f–h). Notice the exposed substrate in (a), (c), and (f). At 800 °C there are almost no particles at the surface. A different situation is seen for 900 °C and 1000 °C, where a homogeneous distribution of NP can be seen in the exposed substrate. Also evident, is the temperature dependence of CNT film thickness.

a lower Ar flux (200 ml/min; Fig. 3). For 1000 °C the average CNTs length was 18.3 μm, while for 900 °C it was only 5 μm and close to 4 μm for 800 °C. This temperature effect, observed before,^{9, 13, 14} has been explained as an increase carbon diffusion rate in iron, which in turn induces a higher rate of incorporation of these atoms into the emerging graphitic structure. At higher temperatures, a greater of C atoms solubility in the Fe-NPs is also expected.¹⁵ These two effects contribute additively to the formation of longer CNTs.

A change in the Ar flow, also influences the ordering of the arrays. More regular arrays are obtained at lower Ar flows. This effect can be seen qualitatively in the SEM images if we compare the top and profile views of the CNTs prepared (1000 °C) with 200 ml/min Ar (Figs. 3g

and 3h) and 500 ml/min (Figs. 2e and 2f). It remains to be seen if these differences are also evident in the electron spectroscopy data. Another consequence of a higher Ar flux is a shorter residence time of the precursor gases in the reaction chamber, implying a smaller availability of carbon atoms, which in turn translates into smaller CNTs. For example, CNT films prepared at 1000 °C with 200, 500, and 1000 ml/min have thickness of 18.3 μm , 13 μm , and 6.5 μm , respectively.

A different effect, which is also temperature dependent, is the location of the Fe-NPs once the synthesis is concluded. Our SEM images for 800 °C (Fig. 3b) show numerous dark speckles at the top of the nanotubes, consistent with a growth mechanism in which the emerging CNTs have pushed the Fe-NP to the top. However, between 900 and 1000 °C most of the Fe-NPs seem to stay attached to the supporting substrate, as shown by Figures 3(e) and 3(h) (900 and 1000 °C). An additional piece of information comes from the on top views shown in Figures 2 and 3. In all of them a section of the turf has been physically removed, to allow a better contrast between the aligned CNTs layer and the substrate. Micrographs for both 900 °C and 1000 °C show a uniform distribution of tiny bright spots, the Fe-NPs, over the section of the substrate in which the CNTs have been removed. This result is in clear contrast with the sample prepared at 800 °C (Fig. 3a), in which the exposed substrate shows almost no Fe-NPs. Our interpretation is that the Fe nuclei formed at 800 °C do not interact as strongly with the substrate. The CNTs grow with the NPs at the top of the tube and remain attached to the CNTs when the films are removed from the substrate. This explanation is consistent with a "tip growth mechanism." Due to a stronger NP-substrate bonding, for 900 °C and 1000 °C, most of the nuclei remain on the substrate instead of the tubes. This second mechanism is known as "base growth."^{7, 17, 18} The interaction strength of the metal NPs with the substrate¹⁷ is then modified by the thermal treatment. Schematic models for both growth modes ("tip and base models") are depicted in Figure 4.

Raman spectroscopy measurements were performed on films of aligned CNTs synthesized at 800 °C, 900 °C, and 1000 °C, with a 200 ml/min argon flux. In general, Raman

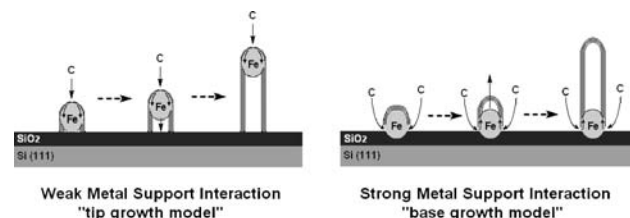


Fig. 4. Schematic model of the CNTs growth mechanisms. Two possible options are depicted: Tip growth and base growth models. The distinctive parameter between both models is the interaction of the metal NP with the substrate. Our results indicate the existence of a transition temperature (T_T) between tip and base growth mode. The transition temperature (T_T) is such that $800\text{ °C} < T_T < 900\text{ °C}$.

spectra from CNTs consist of two dominant features; one in the low frequency range (100–300 cm^{-1}) and the other in the 1500–1600 cm^{-1} range. The low frequency bands are the A_{1g} radial breathing modes (RBM) which are considered a signature for CNTs.¹⁹ This band only appears in SWCNTs and in MWCNTs with a very small inner diameter (few nanometers).²² The bands at the high frequency range correspond to the E_{2g} modes. They originate from the collective tangential C–C stretching (G mode) of an ordered graphitic structure with sp^2 hybridization.^{19, 20} Another typical band appears near 1340 cm^{-1} , this is the so-called disorder-induced band (D band), which originates from the C sp^3 bonds and is mostly related to point defects in the graphitic honeycomb structure^{20, 21} (in pure diamonds (C sp^3) a single peak is expected for these energies). Therefore the ratio of the Raman intensities between the D and G bands provides an indication of the ordering degree of the CNT-walls.^{9, 13, 21}

In our samples, spectral features in the low frequency range are not observed. This confirms that most of the sample consists of MWCNTs. Figure 5 shows the spectra of CNTs in the 1000–2000 cm^{-1} range. In this energy range our MWCNTs samples display two important transitions. The G mode, near to 1585 cm^{-1} and the D band, near 1330 cm^{-1} . If we plot the ratio of the intensities (I_D/I_G : peak height ratios) as a function of growth temperature, we can indirectly verify the evolution of the degree of ordering of CNT-walls. The insert in Figure 5 shows the value of this ratio as a function of growth temperature. From this graph, it is clear that higher synthesis temperatures contribute to the formation of CNT walls with less defects, since I_D/I_G decreases at higher growth temperatures, in agreement with previous reports.^{9, 13, 21} A summary of the relative intensities is also shown in Table I.

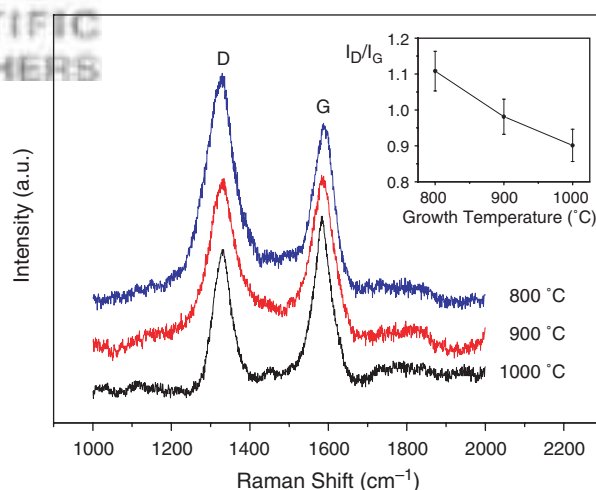


Fig. 5. Raman spectra from MWCNTs films synthesized by pyrolysis of Fe-Pc. The G band corresponds to E_{2g} transition in sp^2 bonds. The D band is related to point defects in graphitic materials. In the insert we show the evolution of the ratio of the amplitudes (I_D/I_G) as a function of growth temperature. A smaller I_D/I_G coefficient is associated with an improved ordering in the graphitic walls.

Table I. Summary of measurements performed on CNTs samples prepared by CVD from FePc. All samples were grown in 20 min. The vertical columns correspond to: Ar flow (Q), temperature of synthesis (T), average height (h), characteristic diameter (D) of the tubes, and the ratio of the Raman intensities for the D and the G bands.

Q_{Ar} (ml/min)	T ($^{\circ}C$)	h (μm)	D (nm)	I_D/I_G
500	900	6	22	
	1000	13	37	
200	800	4	23	1.108
	900	5	26	0.981
	1000	18.3	40	0.901

In order to learn more about the individual characteristics of CNTs, we performed TEM on our samples. The CNTs films were mechanically removed and the resulting powder was dispersed in 2-propanol in an ultrasound bath. The dispersed CNTs were deposited on carbon/copper grids. Figures 6 and 7 show TEM images and diameter frequency histograms of CNTs synthesized with an argon flow of 500 and 200 ml/min, respectively. For each graph more than 100 tubes were included in the statistics. The CNTs synthesized at 900 $^{\circ}C$ (Ar-500 ml/min; Fig. 6) displayed a non Gaussian distribution with a most probable diameter of 22 nm, whereas the ones synthesized at 1000 $^{\circ}C$, have a larger diameter (37 nm) with a broader

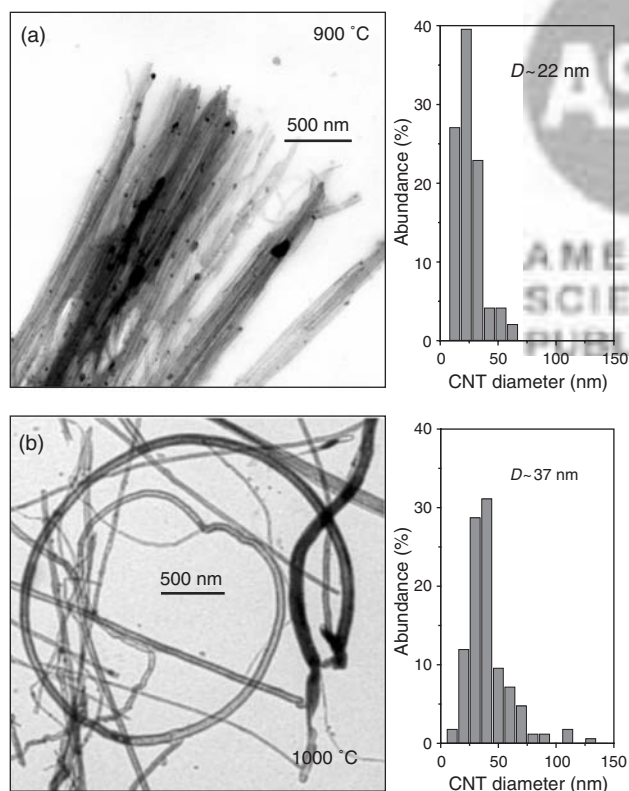


Fig. 6. Bright field TEM micrographs and frequency histograms of dispersed CNTs synthesized at an Ar flux of 500 ml/min; (a) 900 $^{\circ}C$ and (b) 1000 $^{\circ}C$. The most probable diameter (D) of the CNTs prepared at 1000 $^{\circ}C$ is about 68% larger than the ones prepared at 900 $^{\circ}C$. The later also displays a wider spread in the diameter distribution.

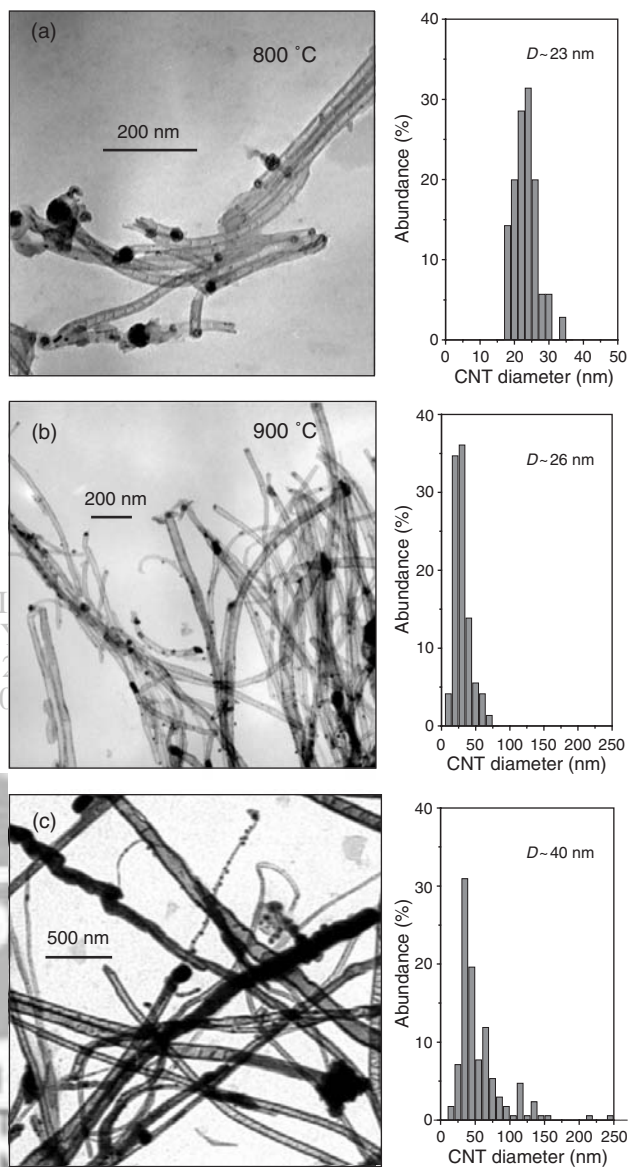


Fig. 7. Bright field TEM micrographs and frequency histograms of dispersed CNTs synthesized with an Ar flux of 200 ml/min at (a) 800 $^{\circ}C$, (b) 900 $^{\circ}C$, and (b) 1000 $^{\circ}C$. The characteristic diameter D of the CNTs prepared at 900 $^{\circ}C$ is only 13% larger than the ones prepared at 800 $^{\circ}C$. Whereas D for CNTs prepared at 1000 $^{\circ}C$ is about 54% larger than those prepared at 900 $^{\circ}C$. This temperature dependence is consistent with measurements done at a higher Ar flux (see Fig. 6).

distribution. For CNTs synthesized with an Ar flux of 200 ml/min (Fig. 7) a similar behavior as a function of temperature was observed. Figure 7a shows a micrograph of CNTs synthesized at 800 $^{\circ}C$ (Ar-200 ml/min), which displays a fairly sharp diameter distribution in the 15–35 nm range, with a characteristic diameter of 23 nm. For the tubes synthesized at 900 $^{\circ}C$ (Ar-200 ml/min) CNTs, a broader distribution (10–75 nm) was obtained, but with a similar characteristic diameter (26 nm). On the other hand, for the same Ar flux, the CNTs synthesized at 1000 $^{\circ}C$ (Fig. 7c) show a fairly different distribution function, with meaningful frequencies from 15 to 150 nm. For this last

sample, some isolated CNTs displayed diameters larger than 200 nm. The characteristic diameter for these tubes is 40 nm, close to twice the value of those synthesized at lower temperatures. For CNTs synthesized with an Ar flux of 500 ml/min (Fig. 6), the same behavior as a function of temperature was observed. CNTs synthesized at 900 °C display a diameter of 22 nm, whereas the ones synthesized at 1000 °C, have a most probable diameter of 37 nm, with a larger dispersion. The temperature dependence on the CNTs diameters seems to be directly related to the iron NPs nucleation process. At higher temperature the iron atoms have a greater tendency to cluster thus forming larger nuclei.²³ Therefore, as the CNTs grow around a larger iron NPs nuclei (or seeds), their final diameter also increases. Unlike temperature, the carrier gas flow (Ar) does not influence considerably the diameter distribution. This conclusion can be readily obtained by comparing the corresponding graphs in Figures 6 and 7.

A detailed analysis of the TEM micrographs reveals two kinds of CNTs structures, cylindrical and bamboo-like. A CNT of cylindrical structure is characterized by a continuous cylindrical wall, with an almost constant diameter and a homogenous wall thickness. However, the bamboo-like structures are tubular but with different size compartments. From the analysis of several micrographs (not all of them shown here), the bamboo shape is the predominant structure for 800 °C (see Fig. 7a), whereas for 900 and 1000 °C the majority of the tubes are cylindrical. Based on this partial result it is tempting to relate the growth mode (tip v/s base growth) with the structure of the walls, but we believe more extensive studies are needed to establish this point and clarify the mechanisms behind the existence of these bamboo type tubes. Figures 8 (a, b, e, and f) show cylindrical and bamboo-like CNTs containing Fe-NPs encapsulated at their ends. Figures 8(c) and 8(g) show CNTs with an open end (which presumably have lost

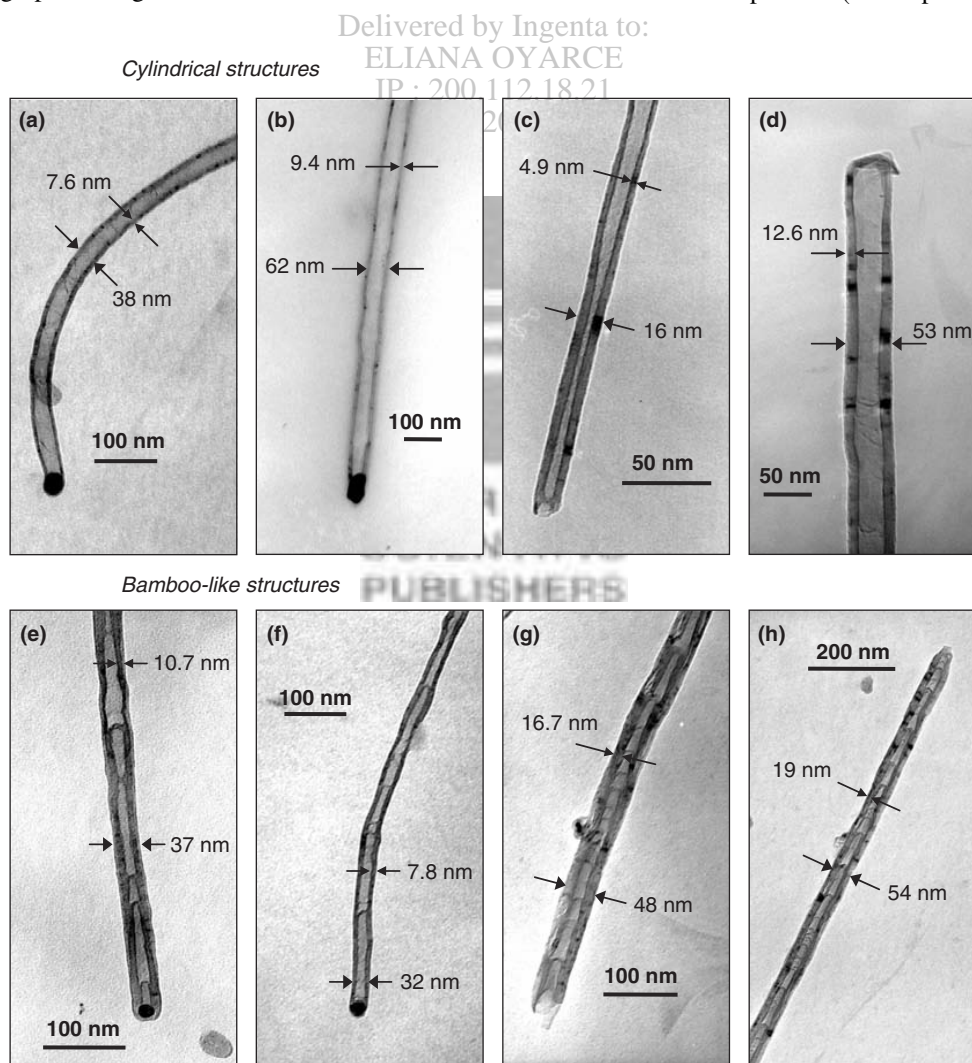


Fig. 8. High magnification TEM micrographs of isolated CNTs showing two types of shapes: Cylindrical (a–d) and bamboo-like (e–h), the later are predominant at low synthesis temperatures. Inserts in the micrographs indicate the outer diameter and the wall thickness of the CNTs. The high contrast at the extreme of the tubes in Figures (a), (b), (e) and (f) is consistent with the presence of Fe-NPs in the CNT's ends. Figures (c) and (g) show CNTs with open ends, while (d) and (h) show capped tips.

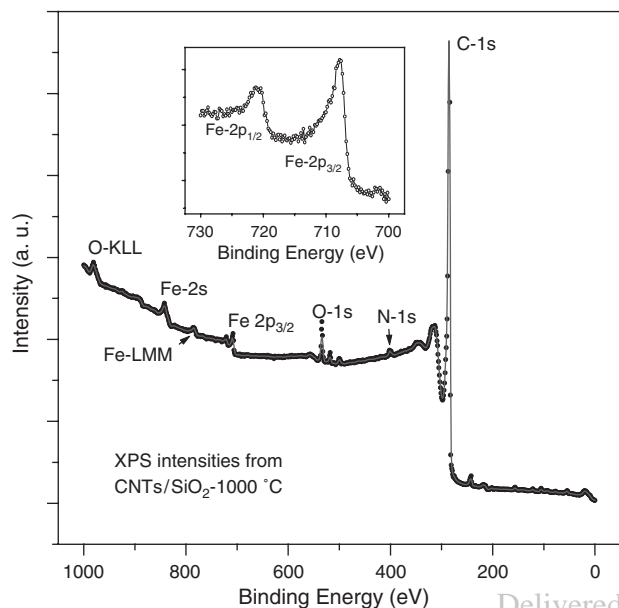


Fig. 9. XPS survey scan spectrum measured on a CNTs film synthesized on SiO_2 at 1000°C . The insert shows the magnified energy region for Fe-2p transitions. Spectra like these were used to establish the relative abundances shown in Table I.

the Fe-NPs), where as in Figures 8(d) and 8(h) the tubes display a closed tip. The apparent CNT wall thickness, as measured by TEM, fluctuates in the range of 5–20 nm. Comparing this thickness with the graphite interlayer spacing (3.35 \AA)²⁴ indicates the CNT's walls have between 15 and 60 graphitic layers.

In order to quantify the Fe content of the samples we performed XPS measurements on the CNTs films grown on SiO_2 . Figure 9 shows the XPS survey spectrum of the 1000°C sample. The insert, in the same figure, shows the characteristic Fe signal for the $2p_{1/2}$ and $2p_{3/2}$ electrons. As expected the most intense peak corresponds to C. In Table II we present a summary of the C/Fe and C/N atomic content ratios for the different CNT films, based on normalized XPS intensities. The C/Fe ratio increases as a function of temperature from 800°C to 1000°C . The smaller ratio for low temperatures is consistent with the Fe-NPs being at the tip of the tubes. These numbers should in general be considered as lower limits for the relative

Table II. Atomic ratio from the top of the CNTs film. Fe 2p and N 1s peaks were measured with respect to C 1s, for films synthesized at 800°C , 900°C , and 1000°C , respectively.

	CNT atomic abundance ratios from XPS	
	C/Fe	C/N
Fe-Pc ⁱ	32	4
800°C	40	
900°C	60	55
1000°C	190	320

ⁱMolecular nominal value, not from spectra.

atomic abundances since the intensity of a particular atomic trace is dependent on the escape depth and the unknown contaminant or dopant spatial distributions in the sample.

The N concentration, as measured by the C/N ratio evolves from the nominal value of 4 in the organometallic precursor, to 55 for the 900°C films and more than 300 for the samples prepared at 1000°C . Based on these numbers most N leaves the CVD system probably as molecular nitrogen. The small proportion of nitrogen still present in the MWCNT-films could be incorporated as substitutional defects in the nanotube walls.⁹ Considering the reduced XPS signal detected from Si, we believe the data presented in Table I is representative of the surface region of the CNTs films, namely, the Fe signal is most likely due to impurities in the region close to the tip of the CNTs instead of the substrate-CNT interface. It is then reasonable to assume only a Fe trace effect on the electron spectroscopy of the MWCNT valence band.

One of the motivations for this work was to explore if FePc based synthesis was appropriate for the production of CNTs to perform electron spectroscopies. Photoemission Spectroscopy (PES) has been the main tool chosen to describe the occupied electronic states in CNTs.²⁵ We have chosen instead Inverse Photoemission Spectroscopy (IPS) which provides complementary information regarding the unoccupied electronic states in these systems. Recent photoemission reports²⁶ on the unoccupied electronic structure of CNTs have proposed the existence of image states of two kinds, spatially extended and localized with respect to the NT axis, but both of them within a small energy

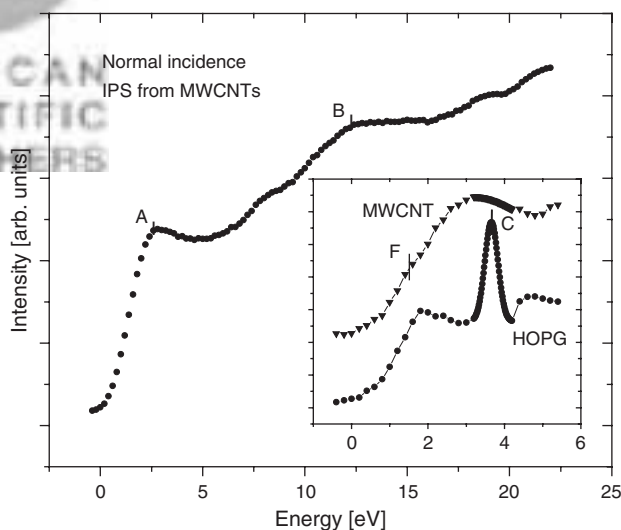


Fig. 10. IPS intensity from a CNT sample synthesized on SiO_2 at 1000°C . The resonance highlighted by A and B have been identified as derived from the π^* and σ^* bands, respectively. The main difference between the HOPG and MWCNTs, occurs in the low energy range ($<5 \text{ eV}$). The lower inset shows a magnification of the IPS spectra from MWCNTs and HOPG. The strong image state feature (C) in graphite is absent from the MWCNT spectrum. Feature F seems to be derived from HOPG.

range below the vacuum level. IPS is certainly the right technique to explore the nature of these resonances.

Figure 10 shows a normal incidence, wide energy scan, IPS spectrum from a MWCNT sample (1000 °C @200 ml/min). The photon intensities are displayed as a function of the incident electron energy. The origin for the energy scale is taken to be at the Fermi level (ϵ_F). For energies beyond this value, the intensity starts to increase fairly rapidly. There are two main resonances in this spectra, one close to 3.0 eV (A) and the other at 12.4 eV (B). We have identified them as being derived from the π^* and σ^* bands respectively, by comparing this particular spectrum to similar measurements performed on graphite.²⁷

For these large diameter tubes, the general belief is that the electronic structure of the tubes is very similar, if not indistinguishable from that of a graphene sheet. This is particularly not true for the unoccupied energy range, where a flat graphene layer, displays a strong resonance close to 3.6 eV (labeled as C in the insert of Fig. 10). This resonance has been identified as being due to an image state; hence its energy and intensity are determined in part by the fact that the surface of graphite is flat. No such resonance is present in the MWCNT samples, at least not with similar intensity or energy as judged from the measured spectrum. A more complete set of IPS data and a detailed analysis of these results will be presented elsewhere.²⁸

One very appealing aspect of these well oriented samples, was the possibility of obtaining angle resolved measurements of the IPS intensity, this would have allowed us to measure the dispersion of the different unoccupied bands along the tubes. Unfortunately our results were not reproducible for different samples prepared under similar conditions. We now believe this is mostly due to the inherent disorder of the top surface (see Fig. 3g) of the tubes array which apparently dominates the spectral IPS response.

4. SUMMARY

The FePc decomposition on a flat substrate like SiO₂/Si(111) can produce MWCNTs which grow preferentially oriented perpendicular to the surface, forming a uniform film. The growth temperature influences both the CNT length and diameter. At higher temperatures it is possible to obtain larger CNTs with wider diameters and walls with better graphitic order. The two main shapes of the CNTs observed are the cylindrical and the bamboo-like structures. Apparently, the carrier gas flux does have an effect in the macroscopic order of the MWCNTs film. Moreover, at higher flows the CNTs lengths are shorter, most likely due to the reduction in the carbon available during the reaction.

From our measurements we can distinguish a transition in the growth mode between 800 °C and 900 °C. For temperatures above 900 °C we observe that most CNTs grow from Fe-NPs rooted on the substrate, following what

is known as a base growth mechanism. On the contrary for 800 °C we observe CNTs grow preferentially with the Fe-NP at the tip end of the tube. The transition in the growth mechanism is apparently related to the temperature dependence of the iron nuclei binding to the substrate. For SiO₂/Si substrates the transition temperature (T_T) is such that 800 °C < T_T < 900 °C. A similar temperature induced transition is observed in the structure of the tube walls. Most of the tubes are cylindrical above 900 °C, while at 800 °C the majority of them are bamboo-like. Preliminary IPS measurements from the high temperature samples show the existence of several resonances in the photon intensity, some of them can be traced back to the graphite unoccupied density of states.

Acknowledgments: This research was possible thanks to the financial support from MECESUP grant FSM 0204 (Postdoctoral Fellowship of R. Segura), Fondecyt 1030198, and Condensed Matter Physics Nucleus grant of ICM, Chile. The authors wish to thank to Dr. E. Couve and Mr. F. Vargas from Universidad de Valparaíso, for the TEM images and Dr. V. Fuenzalida from Universidad de Chile for providing the XPS spectra of our samples.

References and Notes

1. S. Iijima, *Nature* 354, 56 (1991).
2. J. Cumings and A. Zettl, *Science* 289, 602 (2000).
3. A. Nitzan, M. A. Ratner, *Science* 300, 1384 (2003); J. Chung, K. Lee, J. Lee, and R. Ruoff, *Langmuir* 20, 3011 (2004); H. Dai, *Acc. Chem. Res.* 35, 1035 (2002); O. Zhou, H. Shimoda, B. Gao, S. OH, L. Fleming, and G. Yue, *Acc. Chem. Res.* 35, 1045 (2002).
4. V. Bajpai, L. Dai, and T. Ohashi, *J. Am. Chem. Soc.* 126, 5070 (2004); X. Wang, Y. Liu, G. Yu, C. Xu, J. Zhang, and D. Zhu, *J. Phys. Chem. B* 105, 9422 (2001); T. Keller and S. Qadri, *Chem. Mater.* 16, 1091 (2004); B. Wei, R. Vajtai, Y. Jung, J. Ward, R. Zhang, G. Ramanath, and P. Ajayan, *Chem. Mater.* 15, 1598 (2003).
5. A. Cassell, J. Raymakers, J. Kong, and H. J. Dai, *Phys. Chem. B* 103, 6484 (1999); S. Lyu, B. Liu, C. Lee, H. Kang, C. Yang, and C. Park, *Chem. Mater.* 15, 3951 (2003).
6. H. Ago, S. Ohshima, K. Uchida, and M. Yumura, *J. Phys. Chem. B* 105, 43 (2001); R. Seidel, G. Duesberg, E. Unger, A. Graham, M. Liebau, and F. Kreupl, *J. Phys. Chem. B* 108, 1888 (2004).
7. C. Lee and J. Park, *J. Phys. Chem. B* 105, 2365 (2001).
8. S. Huang, L. Dai, and A. W. H. Mau, *J. Phys. Chem. B* 103, 4223 (1999); D. C. Li, L. Dai, S. Huang, A. W. H. Mau, and Z. L. Wang, *Chem. Phys. Lett.* 316, 349 (2000); X. Wang, W. Hu, Y. Liu, C. Long, Y. Xu, S. Zhou, D. Zhu, and L. Dai, *Carbon* 39, 1533 (2001); X. Wang, Y. Liu, and D. Zhu, *Chem. Phys. Lett.* 340, 419 (2001); B. C. Liu, T. J. Lee, S. H. Lee, C. Y. Park, and C. J. Lee, *Chem. Phys. Lett.* 377, 55 (2003).
9. N. S. Kim, Y. T. Lee, J. Park, J. B. Han, Y. S. Choi, S. Y. Choi, J. Choo, and G. H. Lee, *J. Phys. Chem. B* 107, 9249 (2003).
10. V. Vinciguerra, F. Buonocore, G. Panzera, and L. Occhipinti, *Nanotechnology* 14, 655 (2003).
11. (a) Iron(II) Phthalocyanine 97% was purchased from Alfa Aesar, (b) Si(111) *n*(Phos) wafers were purchased from Montco Silicon Technologies Inc. (c) Carbon coated copper grids 150 mesh were purchased from EMS. (d) Deal, B. E. in *Semiconductor Materials and Process Technology Handbook*, William Andrew Publishing (1988).

12. P. Häberle, W. Ibañez, R. Esparza, and P. Vargas, *Phys. Rev. B* 63, 235412 (2001).
13. C. J. Lee, J. Park, Y. Huh, and J. Y. Lee, *Chem. Phys. Lett.* 343, 33 (2001).
14. N. S. Kim, Y. T. Lee, J. Park, H. Ryu, J. H. Lee, S. Y. Choi, and J. Choo, *J. Phys. Chem. B* 106, 9286 (2002); Y. T. Lee, J. Park, Y. S. Choi, H. Ryu, and H. J. Lee, *J. Phys. Chem. B* 106, 7614 (2002); Y. T. Lee, N. S. Kim, S. Y. Bae, J. Park, S. C. Yu, H. Ryu, and J. H. Lee, *J. Phys. Chem. B* 107, 12958 (2003); M. He, S. Zhou, J. Zhang, Z. Liu, and C. Robinson, *J. Phys. Chem. B* 109, 9275 (2005).
15. A. Moiala, A. G. Nasibulin, and E. I. Kauppinen, *J. Phys.: Condens. Matter* 15, 3011 (2003).
16. J. F. AuBuchon, L. H. Chen, A. I. Gapin, D. W. Kim, C. Daraio, and S. Jin, *Nano Lett.* 4, 1781 (2004); S. Takenaka, M. Ishida, M. Serizawa, E. Tanabe, and K. Otsuka, *J. Phys. Chem. B* 108, 11464 (2004).
17. R. T. K. Baker, *Carbon* 27, 315 (1989); K. B. Teo, C. Singh, M. Chhowalla, and W. I. Milne, *Encyclopedia of Nanoscience and Nanotechnology*, edited by B. H. S. Nalwa (2003), Vol. 10, p. 1–22; Y. Ando, X. Zhao, T. Sugai, and M. Kumar, *Materials Today* 7, 22 (2004); L. M. Dell'Acqua-Bellavitis, J. D. Ballard, P. M. Ajayan, and R. W. Siegel, *Nano Lett.* 4, 1613 (2004).
18. W. K. Wong, C. P. Li, F. C. K. Au, M. K. Fung, X. H. Sun, C. S. Lee, S. T. Lee, and W. Zhu, *J. Phys. Chem. B* 107, 1514 (2003).
19. H. Kuzmany, B. Burger, A. Thess, and R. E. Smalley, *Carbon* 36, 709 (1998); J. Hahn, J. H. Han, J. E. Yoo, H. Y. Jung, and J. S. Suh, *Carbon* 42, 877 (2004).
20. F. Tuinstra and J. L. Koenig, *J. Chem. Phys.* 53, 1126 (1970); R. O. Dillon, J. A. Woollam, and V. Katkanant, *Phys. Rev. B* 29, 3482 (1984).
21. M. J. Matthews, M. A. Pimenta, G. Dresselhaus, M. S. Dresselhaus, and M. Endo, *Phys. Rev. B* 59, 6585 (1999); A. Jorio, J. H. Hafner, C. M. Lieber, M. Hunter, T. McClure, G. Dresselhaus, and M. S. Dresselhaus, *Phys. Rev. Lett.* 86, 1118 (2001).
22. Y. Ando, X. Zhao, H. Shimoyama, G. Sakai, and K. Kaneto, *J. Inorg. Mater.* 1, 77 (1999); X. Zhao and Y. Ando, *Jpn. J. Appl. Phys.* 37, 4846 (1998).
23. X. Zhu, C. Blois, K. S. Buchanan, Z. Liu, A. Meldrum, and M. R. Freeman, *J. Appl. Phys.* 97, 10A720 (2005).
24. Y. Baskin and L. Meyer, *Phys. Rev.* 100, 544 (1955).
25. S. Suzuki, Y. Watanabe, T. Kiyokura, K. G. Nath, T. Ogino, S. Heum, W. Zhu, C. Bower, and O. Zhou, *Phys. Rev. B* 63, 245418 (2001).
26. M. Zamkov, N. Woody, B. Shan, H. S. Chakraborty, Z. Chang, U. Thumm, and P. Richard, *Phys. Rev. Lett.* 93, 156803 (2004); B. E. Granger, P. Kral, H. R. Sadeghpour, and M. Shapiro, *Phys. Rev. Lett.* 89, 135506 (2002).
27. I. Schäfer, M. Schlüter, and M. Skibowski, *Phys. Rev. B* 35, 7663 (1987).
28. S. Hevia, W. Ibañez, R. A. Segura, and P. Häberle, to be submitted.

Received: 19 January 2006. Revised/Accepted: 6 February 2006.

